Observation of laser-induced anisotropic changes in the frequency and damping of ion acoustic waves in a laser plasma

J. E. Bernard, H. A. Baldis, and D. M. Villeneuve
Division of Physics, National Research Council of Canada, Ottawa, Ontario, Canada K1A 0R6

A. B. Langdon
Lawrence Livermore National Laboratory, University of California, Livermore, California 94550

W. Rozmus
Department of Physics, University of Alberta, Edmonton, Alberta, Canada T6G 2G7
(Received 20 June 1988)

Temporally and spectrally resolved large-angle Thomson scattering was used to study the frequency and damping of short-wavelength ($k\lambda_{De}\sim 1$) ion acoustic fluctuations in a plasma in the presence of a high-frequency ($\omega_0 > \omega_{pe}$) laser beam. At high laser intensities ($v_{osc}/v_e > 1$), the frequency of the ion acoustic waves which propagated parallel to the electric field of the laser (i.e., parallel to the electron quiver velocity) was observed to be larger than the frequency of the waves which propagated in the perpendicular direction. An increase in the fluctuation amplitude for those waves that propagated parallel to the electric field was observed to be coincident with the shift in the ion acoustic frequency. Both the frequency shift and the increase in the fluctuation amplitude can be explained in terms of the off-resonance ion acoustic decay and the off-resonance oscillating two-stream instabilities. The experimental results are in good agreement with the predictions of theory.

I. INTRODUCTION

A high-intensity electromagnetic wave can produce significant changes in a plasma. Besides heating the plasma through classical absorption, the electromagnetic wave can drive electrostatic plasma fluctuations either directly or indirectly. In particular, parametric processes which involve the generation of large-amplitude electron plasma and ion acoustic waves at the expense of the electromagnetic wave have been studied extensively. In such processes the plasma fluctuation amplitudes can be driven to well above thermal levels and large changes can occur in both the frequency and the damping of these waves.

An intense electromagnetic wave for which $v_{osc}/v_e \gtrsim 1$ [$\mathbf{v}_{osc}=e\mathbf{E}_0/m_e\omega_0$ is the peak oscillation velocity of the electrons in the electric field $\mathbf{E}_0$ of the electromagnetic wave of angular frequency ω_0, and $v_e=(k_B T_e/m_e)^{1/2}$ is the electron thermal velocity] can also change the dispersion relation of plasma fluctuations which are not strongly driven by any parametric process. This was first investigated theoretically by Aliev and Silin[1] for the case $\omega_0 \gg \omega_{pe}$ [$\omega_{pe}=(n_e e^2/m_e\epsilon_0)^{1/2}$ is the electron plasma frequency]. Silin[2] later used a fluid approach with zero thermal motion ($T_e=T_i=0$) to study the situation closer to resonance, $\omega_0\approx\omega_{pe}$. Thermal motions of the electrons and ions were considered in the kinetic treatments of Silin[3] and Sanmartin[4] who studied primarily the cases $\omega_0 \geq \omega_{pe}$ and $\omega_0 \leq \omega_{pe}$, respectively. Besides being of interest in terms of basic plasma physics, changes in the plasma wave fluctuation amplitudes induced by the electromagnetic wave can increase the effective collision rates and lead to enhanced absorption of the electromagnetic wave.

In this paper we report on time-resolved measurements of the effect of a high-intensity laser beam on the frequency and damping rate of thermal level ion acoustic waves. The primary diagnostic used in this experiment to study the ion acoustic waves was time-resolved large-angle Thomson scattering. Thomson scattering from thermal plasma waves has been used extensively in the past as a plasma temperature and density diagnostic in tokamak and other magnetically confined plasmas.[5-7] For these long duration plasmas it has been possible to use multichannel photomultiplier systems to record the temporal changes in the spectrum of the scattered light. In the field of laser plasma interactions, time resolved Thomson scattering using streak cameras has become a standard diagnostic in the study of the very nonthermal plasma fluctuations driven by parametric processes.[8] On the other hand, very few thermal Thomson scattering experiments on laser plasmas have been reported. Most of these experiments have measured the time evolution of the Thomson scattered spectrum in a shot-to-shot manner.[9-11] Recently, we have reported time-resolved Thomson scattering measurements of the electron and ion temperatures obtained with a spectrograph–streak-camera combination.[12] The present work is an outgrowth of these temperature measurements and was motivated by the nonisotropic behavior observed in the spectrum of the Thomson scattered light.[13]

II. THEORY

The plasma dispersion relation in the presence of a long-wavelength electromagnetic wave, as first derived by Silin,[2] is given by

$$1+\frac{1}{\chi_i(\omega)}=\sum_{m=-\infty}^{\infty} J_m^2\left[\frac{\mathbf{k}\cdot\mathbf{v}_{\rm osc}}{\omega_0}\right]\frac{\chi_e(\omega+m\omega_0)}{1+\chi_e(\omega+m\omega_0)}, \quad (1)$$

where $\chi_i(\omega)$ and $\chi_e(\omega)$ are the complex ion and electron susceptibilities, $\mathbf{k}$ and ω are the wave vector and complex frequency of the plasma oscillation, and J_m is the Bessel function of order m. Wave vector $\mathbf{k}$ is much larger than $\mathbf{k}_0$. For the case of either zero laser intensity ($\mathbf{v}_{\rm osc}=\mathbf{0}$) or for waves propagating perpendicular to $\mathbf{E}_0$ ($\mathbf{k}\cdot\mathbf{v}_{\rm osc}=0$), Eq. (1) reduces to the usual field-free plasma dispersion relation, $1+\chi_i(\omega)+\chi_e(\omega)=0$. Equation (1) describes both instabilities and shifts in the frequency of stable ion acoustic waves.

Analytical approximations for the damping and frequency of plasma fluctuations in the presence of an electromagnetic wave have been obtained from Eq. (1) for special plasma conditions[3,4] and more recently exact numerical solutions have been obtained.[14,15] Two regimes with different behavior usually appear in the solutions for $k\lambda_{\rm De}\gtrsim 0.4$,[14-18] where $\lambda_{\rm De}=(k_B T_e\epsilon_0/n_e e^2)^{1/2}$ is the electron Debye length. For the case $\omega_0<\omega_{\rm BG}$, the resulting instability is referred to as the off-resonance oscillating two-stream instability (OTS).[4,17,19] Throughout this paper, $\omega_{\rm BG}$, the Bohm-Gross frequency, is the real part of the frequency of the electron plasma fluctuations determined from the dispersion relation $1+\chi_i(\omega)+\chi_e(\omega)=0$. The usual approximation, $\omega_{\rm BG}^2\approx\omega_{pe}^2+3v_e^2k^2$, is not accurate for values of $k\lambda_{\rm De}\gtrsim 0.4$. For $\omega_0>\omega_{\rm BG}$, the instability is known as the off-resonance ion acoustic decay instability (IAD), or off-resonance parametric decay.[3,17,20] At resonance ($n_e\simeq n_{\rm cr}$) both OTS and IAD can be treated as parametric processes.[16] In IAD the electromagnetic wave decays into an electron plasma wave with frequency $\omega\sim\omega_0$, and an ion acoustic wave with frequency ω_{ia}. Both daughter waves propagate nearly perpendicular to the electromagnetic wave vector (parallel to $\mathbf{E}_0$). In OTS, two electron plasma waves are generated with frequencies $\sim\omega_0$ which propagate in opposite directions. These waves beat together to drive a stationary, zero-frequency ion acoustic fluctuation.

While the growth rates of both instabilities are greatest at resonance (i.e., for plasma densities around critical, $n_{\rm cr}$), at high laser intensities ($v_{\rm osc}/v_e>1$) significant growth can also occur at lower densities in the range $0.5n_{\rm cr}<n_e<n_{\rm cr}$. Both the low-frequency ion acoustic wave and the high-frequency electron plasma wave are driven unstable with the same growth rate and have frequencies shifted from their zero pump field values. In this work we have investigated the growth rate and frequency of only the ion acoustic waves.

In order to illustrate the differences between the off-resonance forms of OTS and IAD we have plotted in Fig. 1 the frequency and damping of the ion acoustic waves as a function of $v_{\rm osc}/v_e$, as obtained from a numerical solution of Eq. (1). The values are normalized by the frequency ω_{ia} and the damping rate γ_{ia} of the ion acoustic wave calculated for zero pump intensity. Note that in Fig. 1(b) $-\gamma/\gamma_{ia}$ is plotted; hence positive values correspond to growth. The plasma parameters for Fig. 1 were chosen to correspond to the interaction of a CO_2 laser beam

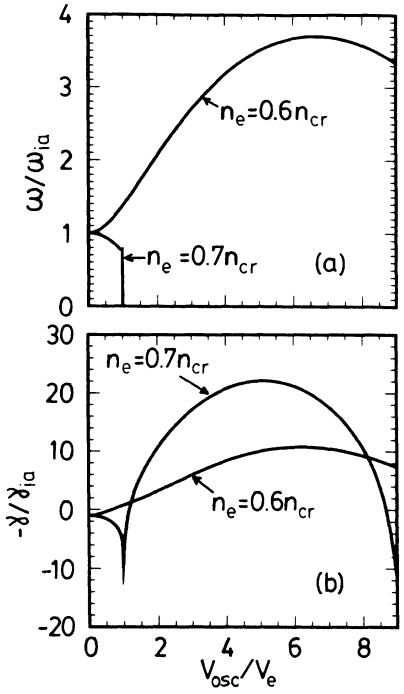

FIG. 1. Numerical solutions of Eq. (1) for (a) the normalized frequency and (b) the normalized damping rate of ion acoustic waves in the presence of a high-intensity electromagnetic wave vs $v_{\rm osc}/v_e$. Values of $-\gamma/\gamma_{ia}$ greater than 0 indicate instability. Carbon plasma: $T_e=T_i=100$ eV, $Z=6$, $k\lambda_{\rm De}=0.38$; CO_2 laser: $\lambda_0=10.6$ μm, $\omega_0=1.78\times10^{14}$ s^{-1}.

($\lambda_0=10.6$ μm, $\omega_0=1.78\times10^{14}$ s^{-1}) with a fully ionized carbon plasma ($Z=6$, $T_e=T_i=100$ eV, $n_{\rm cr}=10^{19}$ cm^{-3}). The wavelength of the ion acoustic wave was chosen such that $k\lambda_{\rm De}=0.38$ (see discussion below concerning Fig. 2). For these conditions, $\omega_{\rm BG}=\omega_0$ at $n_e\simeq 0.63n_{\rm cr}$. Therefore the curves for $n_e=0.6n_{\rm cr}$ correspond to $\omega_0>\omega_{\rm BG}$ and IAD while the curves for $n_e=0.7n_{\rm cr}$ correspond to $\omega_0<\omega_{\rm BG}$ and OTS. For $n_e=0.6n_{\rm cr}$, both the ion acoustic frequency and growth rate increase as $v_{\rm osc}/v_e$ is increased reaching maxima at $v_{\rm osc}/v_e\sim 6$–7. For $n_e=0.7n_{\rm cr}$, the frequency decreases with increasing laser intensity, dropping to zero when the waves become unstable. This instability is therefore nonpropagating and purely growing.

A fluid approach is probably better for obtaining a physical understanding of how the electromagnetic wave can induce a shift in the ion acoustic frequency. This model is valid only for $kv_{\rm osc}/\omega_0\leq 1$ (the amplitude of the electron oscillation is less than the ion acoustic wavelength) and $k\lambda_{\rm De}\lesssim 1$. In the usual first-order derivation of the ion acoustic frequency from the fluid equations, the restoring force for the waves is provided by the pressure gradient ∇p, due to the gradient in density between the wave peaks and troughs. Terms involving $\mathbf{v}\cdot\nabla\mathbf{v}$ in the momentum equations are usually ignored as second order. However, for large electron quiver velocities, $\mathbf{v}_{\rm osc}\cdot\nabla\mathbf{v}_{\rm osc}$ can become significant in the electron equation and its time average (the "ponderomotive force") must be considered along with ∇p in calculating the restoring

force on the ion acoustic waves. The total restoring force and hence the wave frequency can increase or decrease depending on the sign of the $\mathbf{v}_{osc}\cdot\nabla\mathbf{v}_{osc}$ term.

For $\omega_0 > \omega_{BG}$ (IAD) the electron quiver velocity due to the electromagnetic wave for electrons in the wave with wave vector $\mathbf{k}$ is slightly greater for those electrons at the wave crests than for those at the wave troughs. This is because the regions of higher density are closer to resonance ($\omega_{BG}=\omega_0$) since the plasma frequency, ω_{pe}, is greater there. In this case $\mathbf{v}_{osc}\cdot\nabla\mathbf{v}_{osc}$ has the same sign as ∇p and so the restoring force and the wave frequency increase with laser intensity. For $\omega_0 < \omega_{BG}$ (OTS) the quiver velocity of the electrons in the wave with k vector $\mathbf{k}$ is greatest for the electrons at the wave troughs since in this case those electrons are closest to resonance. Therefore, the $\mathbf{v}_{osc}\cdot\mathbf{v}_{osc}$ term decreases the total restoring force and, hence, the wave frequency is expected to decrease with increasing laser intensity.

When the oscillation amplitude of the quivering electrons exceeds approximately one half of the ion acoustic wavelength, $kv_{osc}/\omega_0 \gtrsim \pi$, the electrons oscillate from the wave peaks to the troughs and the fluid model breaks down. Equation (1) does not have the restriction $kv_{osc}/\omega_0 \lesssim 1$. Indeed, the numerical solution of Eq. (1) shown in Fig. 1 exhibits variations in the ion acoustic frequency which can probably be explained in terms of such large oscillation amplitudes. Other aspects of the relationship of the fluid and kinetic approaches are treated in the Appendix.

The simple physical pictures presented so far begin to break down for values of $k\lambda_{De} \gtrsim 0.4$ where the Landau damping of the electron plasma and ion acoustic fluctuations can become very large. For large $k\lambda_{De}$ both the off-resonance IAD and off-resonance OTS instabilities become weaker and in fact the OTS instability ceases to occur. This point is illustrated in Fig. 2 where we have plotted the frequency and growth rates for the ion acoustic fluctuations versus $k\lambda_{De}$ as calculated from Eq. (1). The results for several fixed electron densities are shown. The plasma conditions were chosen to be similar to those encountered in our experiment. Figure 2(b) is almost identical to Fig. 2 in Ref. 15, which was for similar plasma conditions.

For the densities of $0.7\ n_{cr}$ and $0.8 n_{cr}$ both the IAD and OTS instabilities occur. For these densities as $k\lambda_{De}$ is increased from zero, the frequency of the ion acoustic fluctuations increases gradually and reaches a peak value at the point where the IAD instability has its largest growth rate. At $\omega_{BG}=\omega_0$ the growth rate suddenly drops and the frequency falls to zero. For larger values of $k\lambda_{De}$ the OTS instability occurs and the frequency remains at zero. As $k\lambda_{De}$ is increased even further, the growth due to the laser cannot overcome the natural Landau damping of the electron plasma and ion acoustic waves and the instability growth rate begins to fall. At $k\lambda_{De}\sim 0.43$ the OTS growth rate becomes negative (there is a net damping) and the ion acoustic frequency suddenly becomes nonzero. For still larger values of $k\lambda_{De}$ the presence of the electromagnetic wave can cause the ion acoustic frequency to increase and the damping to decrease over the field free values. Such a decrease in the damping, while not actually producing an instability, can in fact lead to an increase in the ion acoustic fluctuation level.[14,21]

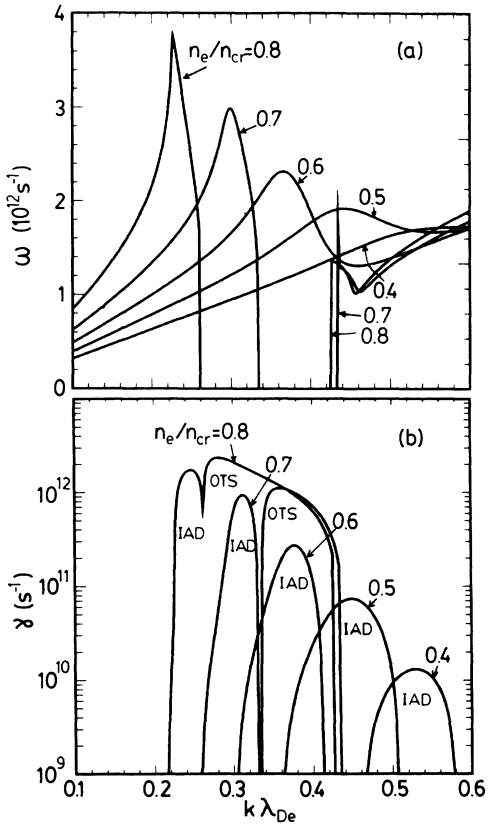

FIG. 2. Numerical solutions of Eq. (1) for (a) the frequency and (b) the growth rate of ion acoustic waves in the presence of a high-intensity laser beam vs $k\lambda_{De}$. Curves for several densities are shown and the regions of IAD and OTS are indicated. Carbon plasma: $T_e = T_i = 100$ eV, $Z=6$; CO_2 laser: $\lambda_0 = 10.6\ \mu$m, $v_{osc}/v_e = 2$.

For lower densities ($n_e \leq 0.6 n_{cr}$), the behavior of the off-resonance IAD instability is similar to that described above. However, the off-resonance OTS instability was not observed in our solutions at the lower densities. Rather, the ion acoustic waves remain damped even for large v_{osc}/v_e. This is in agreement with previous observations by Sanmartin who found that OTS could occur only for $n_e > 0.61 n_{cr}$ [see Eq. (23) of Ref. 4].

III. EXPERIMENTAL DIAGNOSTICS

Since the theory of Thomson scattering can be found in several authoritative works[5,6] only those results pertinent to the present experiment will be summarized here.

The wave vector $\mathbf{k}$ of the plasma fluctuation probed by a particular Thomson scattering optical setup is determined by the Bragg scattering condition

$$\mathbf{k} = \pm(\mathbf{k}_{sc} - \mathbf{k}_{pr}) , \tag{2}$$

where $\mathbf{k}_{pr}$ and $\mathbf{k}_{sc}$ are the wave vectors of the probe and

scattered light, respectively. If $k_{pr} \simeq k_{sc}$ then the magnitude of the probed wave vector is given by

$$k = \frac{4\pi}{\lambda_{pr}} \sin\frac{\theta}{2} , \tag{3}$$

where λ_{pr} is the wavelength of the probe and θ is the angle between the probe and scattered beams. The frequency of the scattered light is red or blue Doppler shifted from the probe frequency by an amount equal to the frequency of the plasma fluctuations,

$$\omega_{sc} = \omega_{pr} \pm \omega . \tag{4}$$

The character of the plasma fluctuations probed in an experiment is determined by the probe wavelength and the scattering geometry. The type of scattering is usually given in terms of the parameter $\alpha = 1/k\lambda_{De}$. For $\alpha \ll 1$, fluctuations are probed whose wavelengths are much less than the Debye length. These fluctuations are heavily damped and the spectrum of the Thomson scattered light is usually Gaussian in shape and reflects the Doppler shift due to scatter from uncorrelated individual electrons. (Because of their much greater mass, the ions scatter much less light than the electrons.) The scattered spectrum is therefore directly related to the electron distribution function.

As α is increased, the wavelength of the probed fluctuations approaches or exceeds the Debye length. These fluctuations are less heavily damped and, in a thermal plasma, resonances start to appear at the Bohm-Gross frequency (electron plasma waves) and the ion acoustic frequency (ion acoustic waves). Note that both these frequencies are defined only for a given wave vector k. These resonances lead to correlations between the electrons in the plasma which in turn lead to peaks in the spectrum of the Thomson scattered light with shifts, according to Eq. (4), of $\pm\omega_{BG}$ (the electron satellites) and $\pm\omega_{ia}$ (the ion feature). The intensities and widths of these spectral peaks are determined by the damping on the associated plasma waves. For values of $\alpha \sim 1$ the electron plasma waves are heavily damped and no electron satellites appear in the scattered spectrum. Only the central ion feature is present and its spectral profile is determined by the electron and ion distribution functions and the electron density. In the present experiment the spectrum of the central ion feature was measured as a function of time for values of $\alpha \sim 1$.

The Thomson scattering spectrum can be calculated from the spectrum of thermal plasma fluctuations. This is usually given in terms of the spectral density function $S(\mathbf{k},\omega)$, which is a measure of the amplitude of fluctuations with wave vector $\mathbf{k}$ and frequency ω. The power scattered into the solid angle $d\Omega$ in the spectral frequency range $\omega_{sc} \rightarrow \omega_{sc} + d\omega_{sc}$, as measured at a point located at position $\mathbf{R}$, is given in terms of the spectral density function by[5]

$$P_{sc}(\mathbf{R},\omega_{sc})d\Omega\, d\omega_{sc} = \frac{P_{pr} r_0^2}{2\pi A} |\hat{\mathbf{s}} \times (\hat{\mathbf{s}} \times \hat{\mathbf{E}}_{pr})|^2 \times n_e V S(\mathbf{k},\omega) d\Omega\, d\omega_{sc} . \tag{5}$$

Here, P_{pr} is the power and A is the cross-sectional area of the incident probe beam, $r_0 = 2.82 \times 10^{-15}$ m is the classical electron radius, and V is the volume of the scattering region defined as the intersection of the probe beam and that part of the plasma imaged by the collection optics. The geometrical factor $|\hat{\mathbf{s}} \times (\hat{\mathbf{s}} \times \hat{\mathbf{E}}_{pr})|^2$, where $\hat{\mathbf{s}}$ is a unit vector in the direction from the scattering volume to point $\mathbf{R}$ and $\hat{\mathbf{E}}_{pr}$ is the unit vector in the direction of the probe polarization, was slightly less than 1 in the present experiment.

From Eq. (5) it can be seen that for a fixed arrangement of the scattering optics the scattered power is determined by the electron density while the shape of the scattered spectrum is determined by the spectral density function. For the case of a stable plasma without the oscillating laser field and with Maxwellian distributions for both the electrons and the ions (we will allow T_e to be different from T_i), $S(\mathbf{k},\omega)$ becomes[5]

$$S(\mathbf{k},\omega) = \frac{(2\pi)^{1/2}}{k v_e} \exp(-x_e^2) \left| 1 - \frac{\chi_e}{\varepsilon} \right|^2 + \frac{(2\pi)^{1/2} Z}{k v_i} \exp(-x_i^2) \left| \frac{\chi_e}{\varepsilon} \right|^2 , \tag{6}$$

where Z is the charge on the ions, $v_i = (k_B T_i / m_i)^{1/2}$ is the ion thermal velocity, and $\varepsilon = 1 + \chi_e + \chi_i$. The effects of the drift velocities of the electrons and the ions $v_{d,e}$ and $v_{d,i}$ are included in the definitions of x_e and x_i,

$$x_e = [(\omega/k) - v_{d,e}]/\sqrt{2} v_e ,$$

$$x_i = [(\omega/k) - v_{d,i}]/\sqrt{2} v_i .$$

Sheffield[5] gives approximate formulas for calculating χ_e and χ_i. Alternatively, they may be calculated directly from the complex error function and the results used to calculate $S(\mathbf{k},\omega)$.

Plots of $\log_{10}[S(\mathbf{k},\omega)]$ as calculated from Eq. (6) are shown in Fig. 3 for values of the parameter α ranging from 0.5 to 5.0. The abscissa is given in terms of the wavelength shift in angstroms to facilitate comparison with experiment. In Fig. 3(a) we have also plotted $\log_{10}[S(\mathbf{k},\omega)]$ for completely uncorrelated electrons in order to illustrate how correlations between the electrons lead to peaks in the scattered spectrum. While as α is increased the scattered spectrum remains dominated by the Doppler broadening from uncorrelated electrons, peaks superimposed on this spectrum appear which result from scatter from those electrons which move at the phase velocity of the plasma fluctuations. According to linear theory the number of those electrons does not increase but rather the correlations between the electrons in the fluctuations lead to constructive interference in the light scattered only from those electrons moving at the wave phase velocity.

In Fig. 3(b) the spectrum of the central ion feature is plotted for a range of values of α. The red- and blue-shifted peaks due to the ion acoustic resonances become prominent features for $\alpha \gtrsim 0.5$. The separation between the two peaks in the ion feature provides a direct measure of the ion acoustic frequency. In addition, several plasma

parameters have almost independent effects on the ion feature and can be determined from a single spectrum. The separation of the two spectral peaks which is equal to twice the ion acoustic frequency is determined largely by the electron temperature [$\omega_{ia} \approx k(ZT_e/m_i)^{1/2}$]. The widths of the peaks as well as the depth of the dip between them are determined by the damping of the waves which in turn is determined by the ratio ZT_e/T_i. Drifts of the ions with respect to the lab frame ($v_{d,i}$) result in a Doppler shift of the entire spectrum. Finally, drifts of the electrons with respect to the ions ($v_{d,e} - v_{d,i}$), as a result for example of a heat flux, lead to a directional dependence in the ion acoustic damping rate. This in turn can lead to an increase in the brightness of one of the spectral peaks. Measurements of the shape of the ion feature therefore can be used to determine T_e, T_i, $v_{d,e}$, and $v_{d,i}$. The electron density can also be determined from the intensity of the ion feature [see Eq. (5)] provided that the scattering optics are calibrated for absolute measurements. This was not done in the present experiment; rather, the plasma density was determined through interferometry.

In the presence of the wave field $\mathbf{E}_0$, Eq. (6) must be replaced. Just as the dispersion function ε appears in the denominator of Eq. (6), a nonlinear dispersion relation corresponding to Eq. (1) appears in the denominator of the modified expressions for the fluctuating density.[21,22] In this way, a theory of scattering from stable plasmas, generalized to include the wave field $\mathbf{E}_0$, would show enhanced scattering when the instability threshold as given by Eq. (1) is approached.

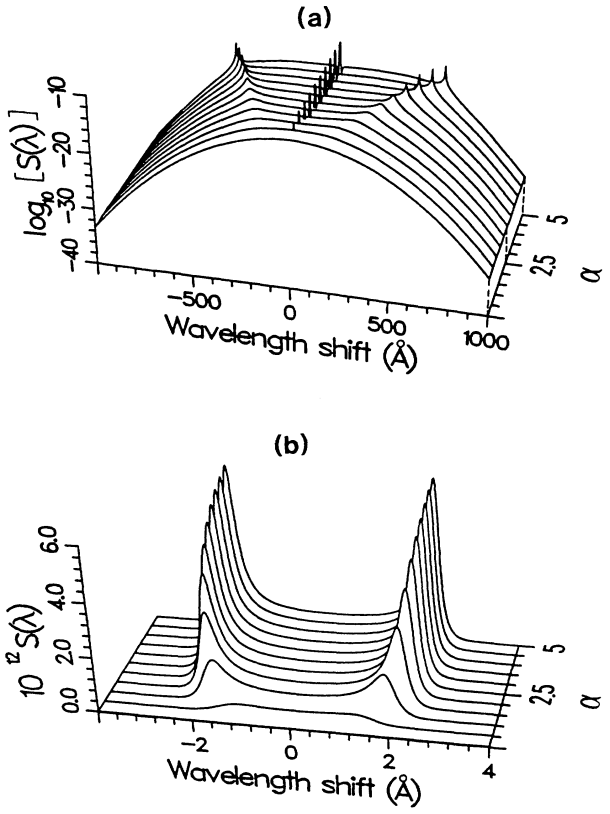

FIG. 3. Theoretical plots of the Thomson scattering spectrum obtained from Eq. (6) for values of α ranging from 0.5 to 5.0. Also shown is the spectrum from completely uncorrelated electrons ($\alpha \to 0$). Carbon plasma: $T_e = T_i = 100$ eV, $Z = 6$, $k = 1.7 \times 10^7$ m^{-1} (n_e varied with α). (a) spectrum showing the central ion feature and the two electron satellites, (b) detail of the central ion feature.

IV. EXPERIMENTAL ARRANGEMENT

The Thomson scattering measurements were performed on the interaction of a CO_2 laser pulse with a preformed carbon plasma. The plasma was produced on the top of a carbon disk 2–3 mm thick and ~45 mm in diameter by a 5–7-J, 20-ns, 1.06-μm laser pulse from a Q-switched Nd:YAG–glass laser system (see Fig. 4, YAG denotes yttrium aluminum garnet). Resulting plasma density profiles, as measured by interferometry, had an approximately Gaussian shape and were cylindrically symmetric about the axis of the 1.06-μm laser beam. The peak density fell off approximately exponentially in the direction antiparallel to the laser beam. The main interaction or pump beam was a horizontally polarized CO_2 laser pulse ($\lambda_0 = 10.6$ μm, 0–35 J) with a roughly triangular temporal shape (0.5-ns rise, 1.5-ns fall) which was focused by an $f/10$ KCl lens onto the side of the preformed plasma as shown in Fig. 4. Typically, the CO_2 laser pulse was delayed 10–20 ns with respect to the glass laser pulse and the interaction region which was located at the intersection of the glass and CO_2 laser beams was 0.3–1.0 mm above the edge of the carbon disk. The measured focal spot had a roughly Gaussian intensity profile but was elongated with $1/e$ radii of 50 and 100 μm. Peak laser intensities ranged up to 2×10^{14} W/cm^2.

A 3–4-ns pulse was switched out of the glass laser pulse, then amplified and frequency doubled to $\lambda_{pr} = 5320$ Å to provide the probe laser pulse for Thomson scattering and interferometry. Synchronization of the plasma production, interaction, and probe laser

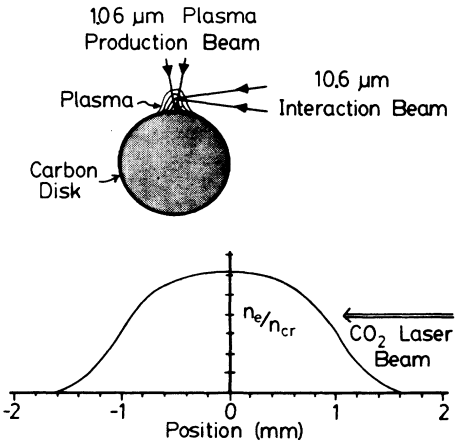

FIG. 4. Experimental arrangement showing the disk target and the plasma production and interaction laser beams. The graph shows a typical plasma density profile along the axis of the CO_2 laser beam.

pulses was accomplished by using the high-voltage pulse from the CO_2 laser switchout Pockels cell to trigger the YAG oscillator Q switch and to switch out the probe pulse.

Electron densities in the preformed plasma were measured on every shot by means of a Mach-Zender interferometer. In the present experiment, the density in the interaction region ranged from $0.3n_{cr}$ to $0.8n_{cr}$. Temporal resolution was limited by the 2–4-ns duration of the probe pulse as well as by the fact that the interferometric fringes were oriented parallel to the CO_2 laser beam and therefore their shape was insensitive to plasma changes caused by the CO_2 laser pulse. However, results of the Thomson scattering measurements, as discussed in Sec. V, indicate that only minor changes to the plasma density occurred during the laser interaction.

The Thomson scattering optical arrangement is shown in Fig. 5. The optics were arranged to make measurements of the Thomson scattered light in two directions in a single shot. The green probe pulse (~ 300 mJ) which was polarized slightly off vertical was focused onto the interaction region to a spot <100 μm in diameter by an $f/10$, 150-mm focal length lens. Thomson scattered light was collected by a second $f/10$, 150-mm focal length lens and focused by a 200-mm focal length lens onto the slit of a spectrograph (1-m, $f/10$, Czerny-Turner, with a 1200-groove/mm grating blazed for 5000 Å). A magnified image of the output spectrum was focused by a cylindrical lens, which was used to cancel the astigmatism introduced by the off-axis focusing of the spectrograph, and a 55-mm focal length lens onto the slit of the streak camera (Hadland Imacon 500). A probe intensity fiducial was split off from the scattering probe beam before the target chamber, sent through an optical delay line, and introduced directly onto the slit of the streak camera, bypassing the spectrograph, by a short piece of optical fiber. The streak records were recorded on negative film and later digitized.

Details of the optical arrangement used for temporally separating the light from the two 90° scattering measurements is shown in Fig. 6(a). The first scattering signal was due to light scattered at 90° with respect to the probe beam, directly into the collection optics. Light which was scattered in the opposite direction was refocused by a confocal mirror system and sent into the same collection optics with an optical delay of 4.0 ns with respect to the first scattering signal. Because of the extremely small scattering cross sections involved, the effect of rescattering of the second signal as it passed through the plasma on its return to the collection optics was negligible.

The wave vectors of the ion acoustic waves probed by the Thomson scattering setup are determined by the wave-vector matching condition [Eq. (2)] and are shown in Fig. 6(b). The first scattering signal was due to light scattered from ion acoustic fluctuations which propagated parallel and antiparallel to the wave vector of the CO_2 pump laser (i.e., perpendicular to the CO_2 laser polarization), while the second scattering signal was due to scatter from ion acoustic fluctuations which propagated perpendicular to the CO_2 laser beam but parallel to its polarization direction. Therefore, for the first scattering signal, $\mathbf{k}\cdot\mathbf{v}_{osc}=0$ and we expect the CO_2 laser pulse to have no direct effect on the Thomson scattering spectrum except through thermal changes in the plasma temperature. However, for the second scattering signal, $\mathbf{k}$ is

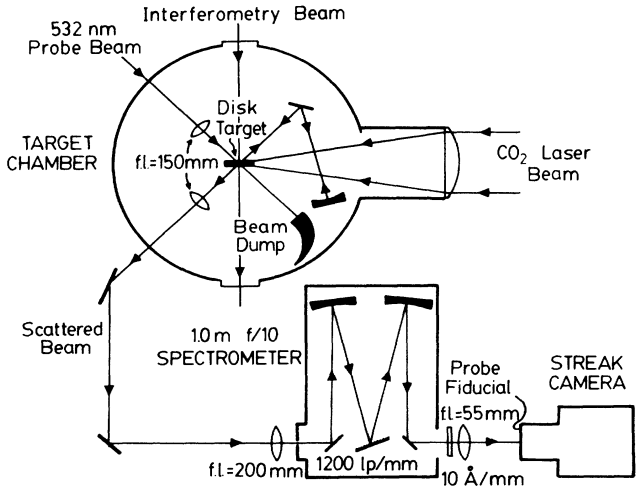

FIG. 5. Thomson scattering optical arrangement.

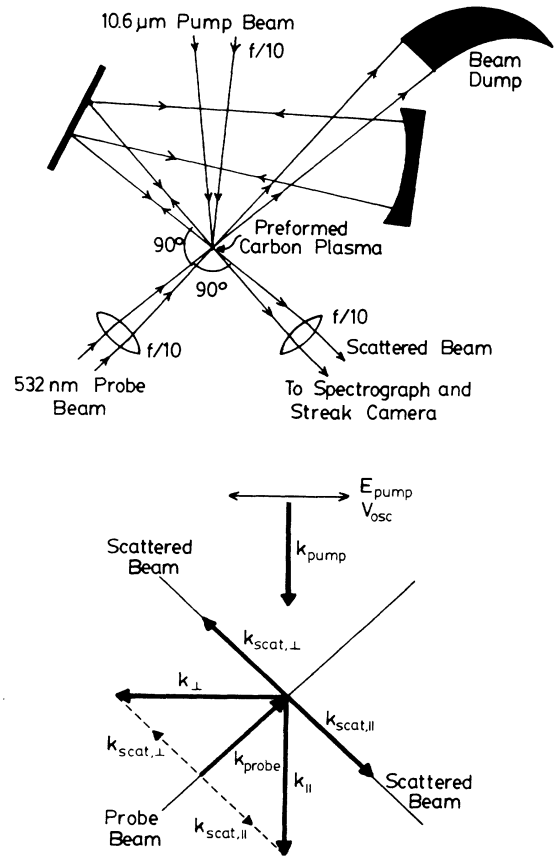

FIG. 6. Details of the Thomson scattering arrangement: (a) the optical setup for simultaneous two-direction 90° scatter, (b) the fluctuation wave vectors probed by the Thomson scattering.

parallel to $\mathbf{v}_{osc}$, and from Eq. (1) we expect the oscillating electrons to cause changes in the ion acoustic frequency and damping rate and hence to lead to changes in the Thomson scattering spectrum.

The scattering optics were aligned with the aid of a 100-μm pinhole located at the interaction region. Final alignment was performed with the target chamber under vacuum and it is estimated that the scattering volumes for the first and second scattering signals overlapped to better than 50 μm. Because of the extremely low scattered light levels (only $\sim 1/10^{11}$ of the probe energy was scattered into the collection optics) great care was taken to optimize the collection efficiency while reducing stray light levels. In order to obtain measurable signals it was necessary to use wide slits on both the spectrograph and the streak camera. This resulted in spectral and temporal resolutions of 0.7 Å and $\lesssim 150$ ps, respectively. The dynamic range of the streak photos was limited to ~ 20 because of the high gain setting of the streak-camera intensifier.

Stray light was reduced in several ways. The probe beam was dumped into a blackened Rayleigh horn, and circular baffles in front of the probe focusing lens and the collection lens limited their fields of view. Because the solid carbon disk was located as little as 300 μm from the scattering region, stray light reflections from the disk were inevitable. Fortunately, by properly orienting the disk and using a small light baffle in contact with its edge it was possible to prevent the reflections from directly entering either set of collection optics. The fact that the scattering region was imaged onto the slit of the spectrograph also reduced the effect of stray reflections since most stray light hit the blades of the slit and did not enter the spectrograph. Finally, although not a problem in this experiment, the temporal dispersion of the streak camera allowed discrimination between the true signal and any light scattered from the chamber walls.

V. RESULTS

The wave vectors probed by the 90° Thomson scattering had magnitudes of $\sim 1.7\times 10^{7}\ \mathrm{m}^{-1}$. Plasma densities in the interaction region were controlled by varying the height of the disk target and in the present experiment ranged from less than $0.3n_{cr}$ to greater than $0.8n_{cr}$ corresponding to k/k_0 ratios in the range from 34 to 63. Therefore, the wave vectors of the probed plasma fluctuations were much larger than those which are driven by parametric processes.[8] For typical plasma temperatures of $T_e \sim 200$ eV, the scattering parameter α ranged from 1.0 to 1.6. The thermal Thomson scattering spectrum is therefore expected to show only the ion feature which, for this range of α's, is influenced to a considerable extent by the plasma density as well as by the electron and ion temperatures.

Streak records of the Thomson scattering spectrum are shown in Fig. 7 for three separate shots. The top part (I) is the spectrum due to ion acoustic fluctuations which

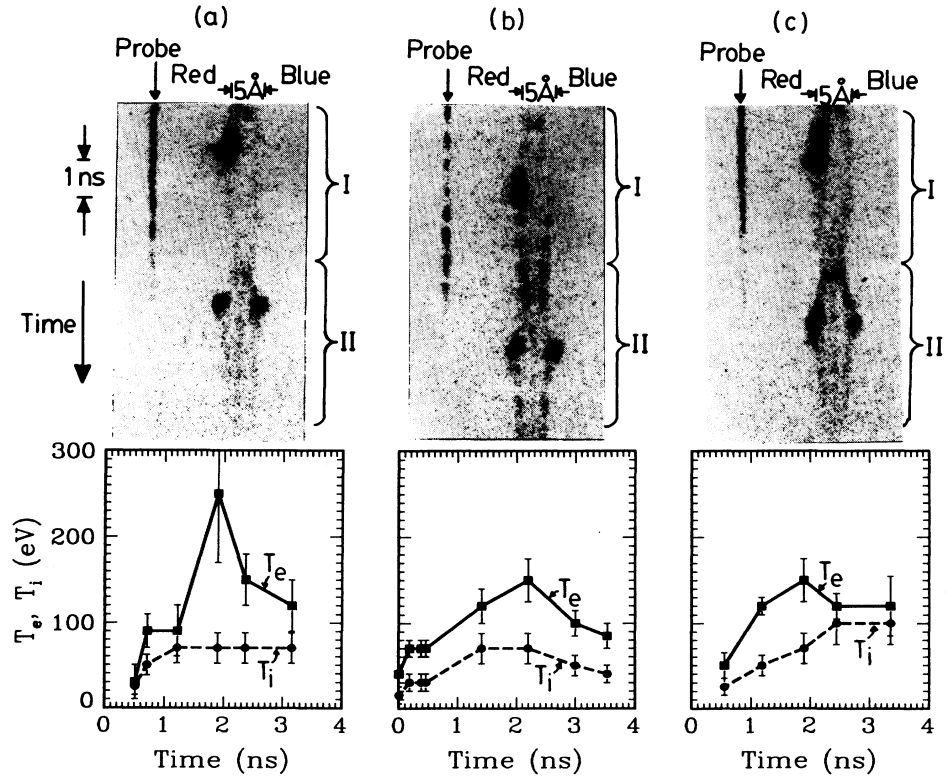

FIG. 7. Streak records showing the spectrally resolved ion feature in the Thomson scattering spectrum. I is the spectrum from fluctuations which propagated perpendicular to $\mathbf{v}_{osc}$ (parallel to $\mathbf{k}_0$). II is the spectrum from fluctuations which propagated parallel to $\mathbf{v}_{osc}$. The graphs show the electron and ion temperature time histories determined from best fits of the upper spectrum (I) by theoretical scattering spectra. (a) $0.6n_{cr}$, 25 J; (b) $0.6n_{cr}$, 23 J; (c) $0.7n_{cr}$, 22 J.

propagated parallel and antiparallel to the wave vector of the CO_2 laser beam. The lower part (II) is the spectrum due to fluctuations which propagated parallel to the electric field of the CO_2 laser beam, i.e., parallel to the electron quiver velocity. Because it was not possible to totally eliminate all the stray light from scatter in both directions, the second scattered spectrum often showed an unshifted peak due to stray light between the two ion feature peaks. Plasma light levels were always below detection threshold.

The probe intensity fiducial is shown along the upper left edge of the streak records. Temporal modulations in the probe intensity are due to mode beating between the longitudinal modes of the YAG oscillator and are much smaller than the sudden intensity modulations observed in the ion feature spectrum. The source of the latter modulations is discussed below.

Since the frequency separation between the two peaks in the ion feature is equal to $2\omega_{ia}$ and $\omega_{ia} \sim (Zk_B T_e/m_i)^{1/2}$, the heating of the plasma during the CO_2 laser pulse and the eventual cooling after the pulse are evident from the streak records. On shots with no CO_2 laser pulse, the scattering spectrum from the preformed plasma was unchanged over the duration of the probe pulse. This indicates that any changes in the preformed plasma conditions occurred slowly and that the probe pulse had negligible effect on the plasma. Therefore any changes during the interaction pulse were solely due to the CO_2 laser.

The streak records were digitized and lineouts made at the times of interest. Plasma conditions were then determined by fitting theoretical Thomson scattering spectra convolved with the instrumental broadening. The top spectrum on the streak records was used for the fitting since theory indicates that this spectrum was unaltered by the presence of the CO_2 laser except through thermal changes in the plasma due to heating. The ion acoustic frequency and damping rate determined from the top spectrum are therefore taken to be equal to the field free values ω_{ia} and γ_{ia}. Possible causes of the sudden enhancements in the red peak of the top spectrum are discussed below.

The fitting of theoretical spectra was accomplished interactively on a computer. Guesses were made for T_e, T_i, $v_{d,e}$ and $v_{d,i}$ and the theoretical spectrum was calculated. The electron density was held fixed at the value determined from interferometry and the average Z of the ions was calculated from T_e using the Saha equation. Parameters were varied until a best fit was obtained. Uncertainties in the fitting results in probable errors in the various parameters of 15% or 10 eV (whichever is larger) for T_e, 25% or 10 eV (whichever is larger) for T_i, 30% for $v_{d,e}$, and 5×10^3 m/s for $v_{d,i}$. The electron and ion temperature time histories determined from the top spectrum on each streak record are shown in Fig. 7.

The relative timing of the CO_2 laser pulse and the streak records was determined only roughly since there was no absolute timing fiducial. The approximate start of the laser pulse was signaled by an increase in the electron temperature. Simulations[12] have shown that the maximum electron temperature should occur very near to the time of peak laser intensity. However, the timing determined from this method did not agree with that determined from the onset of heating. The uncertainty in the timing of the CO_2 laser pulse determined from this discrepancy is estimated for the present experiment to be approximately $\pm 0.3-0.5$ ns.

VI. DISCUSSION

Except for the brief periods of enhanced scatter, the intensity of the ion feature spectrum before and during the CO_2 laser pulse was almost unchanged. Therefore the plasma fluctuation levels remained at their low thermal levels during the interaction pulse. On some shots where no sudden asymmetric increase in the intensities of two peaks of the first spectrum was observed, a slight decrease in the overall intensity was noted as the electron temperature increased. This behavior can be almost entirely accounted for by the decrease in $S(\mathbf{k},\omega)$ as the electron temperature was increased. [$S(\mathbf{k},\omega)$ decreases by $\sim 50\%$ between $T_e = 50$ eV and $T_e = 150$ eV]. Therefore we conclude that any changes in the plasma density during the interaction pulse either due to further ionization or hydrodynamic motion were small and that the density measured by interferometry was a reasonable estimate of the actual density during the interaction.

A. Frequency shift

From the streak records shown in Fig. 7 it can be seen that the maximum separation of the two spectral peaks was greater in the second spectrum (II) than in the first (I). This implies that the ion acoustic frequency was greater for those fluctuations which propagated parallel to $\mathbf{v}_{osc}$ than for those that propagated perpendicular to $\mathbf{v}_{osc}$ (parallel to $\mathbf{k}_0$). Since T_e is roughly proportional to the square of the spectral peak separation (at least for the case of zero laser intensity), this difference, if interpreted as due to a directional dependence in the electron temperature, would imply a very nonisotropic electron distribution function. It is difficult, however, to explain how the rapid oscillation of the electrons in the field of the laser could lead to two different "thermal" distributions with different temperatures. The electron-electron Maxwellianization time[23] for a plasma at a temperature of $T_e = 150$ eV and a density of $n_e = 5\times10^{18}$ cm^{-3} is 10–20 ps. Since the 90° deflection time[23] for electrons for the same conditions is less than 1 ps, the electron distribution function should isotropize before two thermal distributions with different temperatures can develop. We have proposed[13] instead that the difference between the two scattering spectra was directly due to a directional dependence in the ion acoustic frequency, as discussed in the theory section, rather than a nonisotropic electron temperature. While the electron distribution function in the laboratory frame is still required to be highly nonisotropic and nonthermal as a consequence of the oscillating field of the laser (the distribution function in the direction of $\mathbf{E}_0$ is double peaked), the distribution function in the

oscillating frame is assumed to be isotropic and Maxwellian.

In Fig. 8 we have plotted the ratio of the peak measured ion acoustic frequency for fluctuations which propagated parallel and perpendicular to $\mathbf{v}_{osc}$ versus the peak value of v_{osc}/v_e. Here, v_{osc} is determined from the spatially averaged laser intensity incident on a spot 100 μm in diameter with the assumption of no refraction or deterioration of the beam. The results from shots with peak electron temperatures between 50 and 250 eV and plasma densities in the ranges $0.45n_{cr} \leq n_e \leq 0.6n_{cr}$ and $0.6n_{cr} \leq n_e \leq 0.75n_{cr}$ are included. The results show no strong density dependence. This appears surprising since it is expected that at the lower densities off-resonance IAD should occur for which the frequency ratio is greater than 1, while at the higher densities, off-resonance OTS should occur for which the frequency ratio is equal to zero. However, as can be seen from Fig. 2(a), a nonzero frequency ratio occurs at the higher densities for both small values of $k\lambda_{De}$, at which off-resonance IAD occurs, and for large values of $k\lambda_{De}$ where the ion acoustic wave remains damped. Only in the narrow range of $k\lambda_{De}$ values where OTS occurs is the frequency ratio equal to zero.

Since λ_{De} increased rapidly as the plasma was heated by the CO_2 laser, the value of $k\lambda_{De}$ rapidly passed through the range favorable to OTS. For example, just prior to the CO_2 laser pulse, the electron temperature was $\sim$40 eV resulting in $k\lambda_{De} \sim 0.3$ for $n_e = 0.7n_{cr}$. Therefore, provided the laser intensity was sufficient, IAD occurred and the frequency ratio was greater than 1. Even for laser intensities below the IAD threshold, the ion acoustic frequency is expected to shift to larger values (see Fig. 1). By the time the plasma temperature had increased to only 85 eV the value of $k\lambda_{De}$ had reached 0.43 and the region of OTS had been passed. For higher temperatures, although the waves remain damped, the frequency ratio could again be greater than 1. Since the measured peak electron temperatures were higher than 100 eV, we conclude that the frequency ratios greater than one measured for $n_e > 0.6n_{cr}$ were likely due to the "instability" operating in either the IAD or this latter, damped regime.

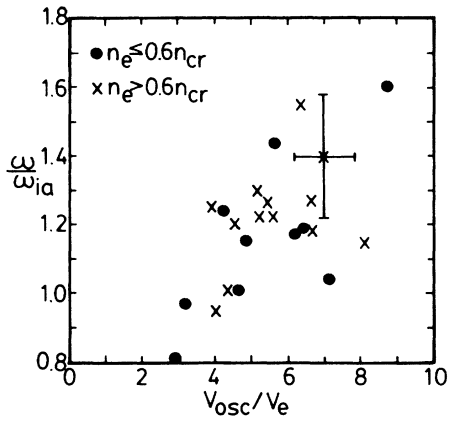

FIG. 8. Measured ratio of ion acoustic frequencies for fluctuations propagating parallel and perpendicular to $\mathbf{v}_{osc}$ vs the ratio of the peak electron quiver velocity to the electron thermal velocity. Plasma densities ranged from $0.45n_{cr}$ to $0.75n_{cr}$ and peak electron temperatures ranged from 50 to 250 eV. The error bars shown represent the typical statistical uncertainties in the measurements.

B. Enhanced fluctuations

As can be seen from the lower spectra in the streak records shown in Fig. 7, a sudden enhancement in the scattered intensity occurred coincident with the largest shift in ion acoustic frequency. In fact, often the spectral peak separation remained small until the time of the enhancement when the peaks suddenly separated [see Fig. 7(a)]. This enhancement in the scattered light intensity is due to an increase in the ion acoustic fluctuation level above the normal thermal level. We interpret this change in the fluctuation amplitude to be due to either a decrease in the ion acoustic damping rate or an instability in the waves, both of which are caused by the CO_2 laser and are associated with the frequency shift through the off-resonance IAD and OTS instabilities.

The scattered light level during the period of enhancement was measured to increase typically by a factor of less than 20 (approximately the dynamic range of the streak camera). Since the scattered intensity is proportional to $S(\mathbf{k},\omega)$ [see Eq. (5)] and $S(\mathbf{k},\omega)$ is proportional to[5,6] $|\tilde{n}_e(\mathbf{k},\omega)|^2/n_e$, where $\tilde{n}_e(\mathbf{k},\omega)$ is the Fourier component of the fluctuating electron density with wave vector $\mathbf{k}$ and frequency ω, the presence of the laser caused an enhancement of only 4–5 times in the fluctuation amplitude. This level of enhancement is much less than that observed in a previous experiment[14,24] where the enhancement in the fluctuation level ranging from 2 to 10^4 times were observed. (However, for $k\lambda_{De}$ values similar to those encountered in the present experiment the enhancement levels were comparable.) In that experiment the enhanced scattering levels were also attributed to an increase in the ion acoustic fluctuation level driven by the off-resonance OTS and IAD instabilities. However, they observed that the level of enhancement was the same both in and out of the plane of polarization of the unpolarized pump laser. While we observed enhanced fluctuations propagating both parallel and perpendicular to the pump polarization ($\mathbf{E}_0$), our spectrally resolved measurements have revealed that the character of the enhancement was very different in the two directions. Whereas in the direction parallel to $\mathbf{E}_0$ both spectral peaks were enhanced as predicted for the OTS and IAD instabilities, in the direction perpendicular to $\mathbf{E}_0$, only the red spectral peak was enhanced while the blue peak actually faded. Because of this difference in behavior and the fact that theory predicts that off-resonance IAD and OTS should have no effect on ion acoustic waves propagating perpendicular to $\mathbf{E}_0$, we conclude that some other mechanism(s) besides IAD and OTS was responsible for the enhancement in the ion acoustic waves which propagated perpendicular to $\mathbf{E}_0$.

The enhancement of the red peak and the fading of the blue peak shown in the top spectra of the streak records

of Fig. 7 correspond to an increase (decrease) in the fluctuation amplitude of those ion acoustic waves which propagated antiparallel (parallel) to the CO_2 laser wave vector $\mathbf{k}_0$. Theoretical Thomson scattering spectra[5,6,12] can be fitted to the experimental spectra by assuming simply a drift of the electrons through the plasma in the direction antiparallel to $\mathbf{k}_0$. Such a drift leads to a difference in the slope of the electron distribution function at the ion acoustic velocities for waves which propagate parallel and antiparallel to $\mathbf{k}_0$. This in turn leads to differences in the Landau damping rates and hence a difference in the fluctuation amplitude and scattered intensity. We therefore believe that in the present experiment, the asymmetric behavior observed in the enhancement of top spectrum of Fig. 7 can be attributed to an electron drift, probably driven by a heat flux.[25]

C. Comparison to theory

A detailed comparison of the time histories of the frequency ratios as measured from the three streak records shown in Fig. 7 and those predicted from theory are shown in Fig. 9. Calculated time histories of the corresponding damping rate ratios are also plotted. The period of enhancement of the bottom spectra on the streak records is indicated. The theoretical curves were calculated using the measured time histories of the electron and ion temperatures shown in Fig. 7. The electron density and the laser intensity as well as the time of the start of the laser pulse were varied in order to obtain a best fit to the experimental points. A triangular pulse with a 0.5-ns rise time and 1.5-ns fall time was used to approximate the temporal shape of the CO_2 laser pulse. The start of the pulse was taken to be approximately the time at which the electron temperature started to rise from its value in the preformed plasma. As has already been mentioned, uncertainties in the actual temporal shape of the laser pulse lead to an uncertainty in the timing between the laser and the streak photos of $\pm 0.3-0.5$ ns.

Qualitatively, the behavior of the frequency and damping predicted from theory is very similar to that seen in the experiment. Both theory and experiment show an increase in the ion acoustic frequency for those waves which propagated parallel to $\mathbf{v}_{osc}$. The sudden enhancement in the scattered intensity at the time of the largest frequency shift corresponds to the period of growth or decreased damping seen in the theoretical calculations. The theoretical curves plotted in Fig. 9 are quantitative best fits to the experimentally measured frequency ratio. The electron density and peak laser intensity used in the fitting are indicated in the caption to Fig. 9. In addition, we have listed the experimentally measured electron density at the interaction region in the preformed plasma and the peak CO_2 laser intensity, spatially averaged over the central 100-μm focal spot. Consideration of probable corrections and experimental uncertainties indicates that the quantitative agreement between the measured and best-fit values for the density and intensity is much better than indicated by these numbers.

The plasma density required to give a best fit was in all cases $\sim 0.1n_{cr}-0.2n_{cr}$ smaller than that measured for the preformed plasma. Although, as previously noted, the scattering results do not show any evidence of large changes in the electron density in the interaction region during the CO_2 laser pulse, a change in the density of only 20–30% would probably have been difficult to detect because of the changes in the scattered intensity due to other effects such as electron drifts and changes in $S(\mathbf{k},\omega)$ due to plasma heating. For this reason and also

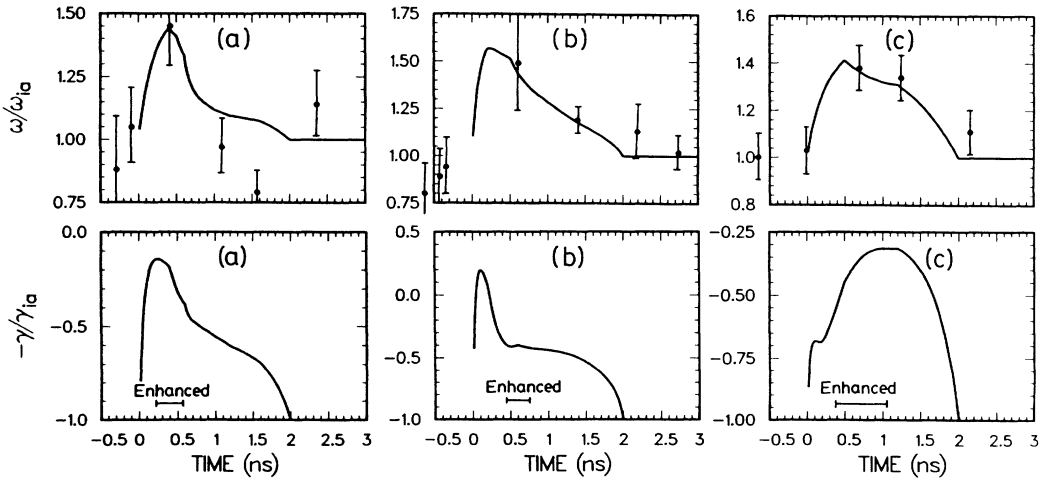

FIG. 9. Best-fit time histories of the frequency ratio and the negative of the damping ratio for ion acoustic waves which propagated parallel and perpendicular to $\mathbf{v}_{osc}$ as calculated from Eq. (1) for measured electron and ion temperatures. Parts (a), (b), and (c) correspond to the streak records shown in parts (a), (b), and (c), respectively, of Fig. 7. The plotted points are from direct measurements of the frequency ratio as measured from the streak records of Fig. 7. The period of enhancement of part II of the streak records is shown. (a) Experimental: $n_e=0.6n_{cr}$, $I=1.1\times10^{14}$ W/cm^2: best fit: $n_e=0.5n_{cr}$, $I=0.3\times10^{14}$ W/cm^2. (b) Experimental: $n_e=0.6n_{cr}$, $I=1.0\times10^{14}$ W/cm^2; best fit: $n_e=0.5n_{cr}$, $I=0.5\times10^{14}$ W/cm^2. (c) Experimental: $n_e=0.7n_{cr}$, $I=1.0\times10^{14}$ W/cm^2; best fit: $n_e=0.5n_{cr}$, $I=0.6\times10^{14}$ W/cm^2.

because of uncertainties in the interferometry and Abel unfolding process, we consider the density required for a best fit to be within experimental uncertainty of the measured density.

The laser intensity required for a best fit was about a factor of 2–4 smaller than that expected from the measured focal spot size and the incident laser energy. However, since the CO_2 laser beam propagated at an oblique angle to the density gradient in the preformed plasma, the beam was refracted away from the region probed by the Thomson scattering. Measurements of burn marks produced by the CO_2 laser beam after passing through the plasma, as well as numerical ray tracing, have indeed shown considerable defocusing and deflection. The discrepancy between the measured temporal behavior of the electron temperature and that predicted by numerical simulations[12] is also evidence for beam refraction. Therefore, we believe that refraction can probably account for the reduction in the laser intensity required in order to achieve quantitative agreement between the experiment and theory.

The growth rates predicted by theory are approximately $10^{11}\ s^{-1}$. The fluctuation level e-folding time is therefore only ~ 10 ps and it is expected that the enhancement in the fluctuation level should be much higher than the 4–5 times observed in the experiment. The predicted growth rates may be too large because of an incorrect choice of the plasma and laser parameters. Since the conditions were such that the laser frequency was very close to the Bohm-Gross frequency, a small change in the plasma density or laser intensity could greatly change the growth rate or have even caused the instability to disappear and the enhancement to have been due to reduced damping alone. It has also been suggested[15] that since for the off-resonance IAD instability two electron plasma waves are present, these waves can couple together and drive the second harmonic of the unstable ion acoustic wave. Such a process can act as a source of enhanced damping and possibly saturate the instability.

Finally, both off-resonance IAD and OTS are expected to produce unstable electron plasma waves which grow at the same rate as the ion acoustic waves studied in this experiment. Since these waves are normally quite heavily damped, any resonances associated with the instability would likely be quite broad [see Fig. 3(a)]. In addition, since for our plasma parameters, more total light is scattered into the Thomson scattering ion feature than into the electron satellites,[5] and the ion feature was enhanced by only ~ 20 times, the electron satellites probably remained below the detection threshold. A brief search was made for enhanced electron plasma waves and in accordance with the points above, no signals above stray light levels were observed.

VII. CONCLUSIONS

We have compared the frequency and damping rates of ion acoustic waves which propagate parallel and perpendicular to the electric field of a high intensity polarized laser beam. In agreement with the predictions of theory, we have observed an intensity dependent increase in the ion acoustic frequency as well as an increase in the fluctuation amplitude of ion acoustic waves which propagated parallel to the laser electric field, i.e., in the direction of $\mathbf{v}_{osc}$. Observed ratios of the ion acoustic frequencies for waves which propagated parallel and perpendicular to $\mathbf{v}_{osc}$ were as large as 1.6 while the enhanced fluctuations were 4–5 times thermal levels. Time histories of the measured frequency ratio and the fluctuation level show good qualitative agreement with the temporal behavior predicted by theory. Reasonable quantitative agreement is also obtained if corrections due to refraction and defocusing of the laser beam as it passed through the plasma are applied to the laser intensity.

Although the frequency shifts and observed changes in the fluctuation levels can be caused by both the off-resonance IAD and the off-resonance OTS instabilities, Thomson scattering constraints and beam refraction led to experimental conditions which were more favorable to the detection of IAD than OTS. Conditions favorable to off-resonance OTS, if they existed at all, probably occurred only for a short time while the plasma temperature was changing rapidly. Considerable changes in the present experiment would be necessary to study this instability in detail.

ACKNOWLEDGMENTS

We would like to acknowledge valuable discussions with W. L. Kruer, T. W. Johnston, and F. Brunel, and the technical support of R. Benesch. We would also like to thank A. Avery and J. Watton for operating the CO_2 laser.

APPENDIX

Here we derive expressions for the frequency shift in various limits from a fluid theory and from the Silin dispersion relation, Eq. (1). A fluid theory for parametric instabilities yields[26]

$$\frac{\omega^2}{\omega_{pi}^2}=\frac{k^2\lambda_{De}^2}{1+k^2\lambda_{De}^2}+\left[\frac{kv_{osc}}{2}\right]^2\left[\frac{(\hat{\mathbf{k}}_-\cdot\hat{\mathbf{E}}_0)^2}{\omega_-^2-\omega_{pe}^2(1+3k_-^2v_e^2/\omega_-^2)}+\frac{(\hat{\mathbf{k}}_+\cdot\hat{\mathbf{E}}_0)^2}{\omega_+^2-\omega_{pe}^2(1+3k_+^2v_e^2/\omega_+^2)}\right], \tag{A1}$$

where ω_{pe} and ω_{pi} are the electron and ion plasma frequencies, ω and $\mathbf{k}$ are the frequency and wave vector of the ion sound wave, and $\hat{\mathbf{k}}_\pm$ and $\hat{\mathbf{E}}_0$ are *unit* vectors in the directions $\mathbf{k}_\pm\equiv\mathbf{k}_0\pm\mathbf{k}$ and $\mathbf{E}_0$. The electromagnetic terms have been dropped; because $k\gtrsim 3k_0$, the solenoidal fields at $\omega_\pm\equiv\omega_0\pm\omega\simeq\omega_0$, $\mathbf{k}_\pm\simeq\pm\mathbf{k}$ are farther off resonance than are the irrotational fields. For $k\lambda_{De}\lesssim 1$, $k\gg k_0$, and $\omega_0-\omega_{pe}\gg\omega_{pe}(kv_e/\omega_0)^2$, we find that the effective electron temperature for ion sound waves is increased by the factor

$$\left[\frac{\omega}{kc_s}\right]^2 = 1+\frac{v_{\rm osc}^2}{2v_e^2}\frac{\cos^2\theta}{n_{\rm cr}/n_e-1}$$
$$= 1+\frac{(kv_{\rm osc}/\omega_0)^2}{2(k\lambda_{\rm De})^2}\frac{\cos^2\theta}{1-n_e/n_{\rm cr}}\ , \qquad \text{(A2)}$$

where $c_s=(ZT_e/m_i)^{1/2}$ is the isothermal sound speed, ω/k is the (modified) sound speed, $v_e^2=k_BT_e/m_e$, $v_{\rm osc}$ is the (peak) electron oscillation velocity in the electric field $\mathbf{E}_0$ of the 10.6-μm laser light, θ is the angle between $\mathbf{k}$ and $\mathbf{E}_0$, and $n_e/n_{\rm cr}$ is the electron density relative to critical density. Thus the sound wave dispersion will seem to indicate an enhanced anisotropic electron temperature.

In the experiment, $n_e/n_{\rm cr}=0.5$–0.8, $v_{\rm osc}/v_e\sim 2$–8, and $k/k_0\gtrsim 33$. These lead to $k\lambda_{\rm De}\sim 1$, $kv_{\rm osc}/\omega_0$ is not small, and $\omega_0/kv_e\sim 1$. Any of these conditions invalidates the derivation of Eq. (A2), which predicts too large an effect. Keeping the assumption $k_0\ll k$, we can use Eq. (1), which applies for arbitrary $kv_{\rm osc}/\omega_0$, with kinetic electron and ion response.

With the orderings $kv_i\ll\omega\ll kv_e\ll\omega_0$, we have $-\chi_i\simeq\omega_{pi}^2/\omega^2$, $\chi_e(\omega)\simeq(k\lambda_{\rm De})^{-2}$, and $\chi_e(\omega_m)=-\omega_{pe}^2/\omega_m^2$. Equation (1) becomes

$$\frac{\omega^2}{\omega_{pi}^2}=\frac{k^2\lambda_{\rm De}^2+[1-J_0^2(kv_{\rm osc}/\omega_0)]}{1+k^2\lambda_{\rm De}^2}$$
$$+2\sum_{m=1}^{\infty}\frac{J_m^2(kv_{\rm osc}/\omega_0)}{(m\omega_0/\omega_{pe})^2-1}\ . \qquad \text{(A3)}$$

One cannot simply combine linearly the pressure contributions of v_e^2 and $v_{\rm osc}^2$, as in Eq. (A2). The independent parameters include at least $(k\lambda_{\rm De})^2$ and k/k_0, in addition to $(v_{\rm osc}/v_e)^2$ and $n_e/n_{\rm cr}$. In Eq. (A3), note that $1-J_0^2$ and every term in the summation are positive, so the sound frequency is *always increased* by the presence of the laser light, in this approximation.

In the limits of cold plasma and low density (small ω_{pe}^2/ω_0^2), Equation (A3) reduces to $\omega^2=\omega_{pi}^2[1-J_0^2(kv_{\rm osc}/\omega_0)]$; this is Eq. 1.14 of Aliev and Silin,[1] who call this effect *anisotropic sound.* Kaw and Dawson[27] also consider alteration of sound wave dispersion, but close to critical density and in the small $kv_{\rm osc}/\omega_0$ limit.

[1]Yu. M. Aliev and V. P. Silin, Zh. Eksp. Teor. Fiz. **48**, 901 (1965) [Sov. Phys.–JETP **21**, 601 (1965)].

[2]V. P. Silin, Zh. Eksp. Teor. Fiz. **48**, 1679 (1965) [Sov. Phys.–JETP **21**, 1127 (1965)].

[3]V. P. Silin, Zh. Eksp. Teor. Fiz. **51**, 1842 (1966) [Sov. Phys.–JETP **24**, 1242 (1967)].

[4]J. R. Sanmartin, Phys. Fluids **13**, 1533 (1970).

[5]J. Sheffield, *Plasma Scattering of Electromagnetic Radiation* (Academic, New York, 1975).

[6]D. E. Evans and J. Katzenstein, Rep. Prog. Phys. **32**, 207 (1969).

[7]N. C. Luhman, Jr., and W. A. Peebles, in *Laser Handbook,* edited by M. Bass and M. L. Stitch (North-Holland, Amsterdam, 1985), Vol. 5, p. 455.

[8]H. A. Baldis, D. M. Villeneuve, and C. J. Walsh, Can. J. Phys. **64**, 961 (1986).

[9]S. R. Kimberlin, P. W. Chan, R. C. Hazelton, and E. J. Yadlowsky, J. Appl. Phys. **49**, 2700 (1978).

[10]D. R. Gray, J. D. Kilkenny, M. S. White, P. Blyth, and D. Hull, Phys. Rev. Lett. **39**, 1270 (1977).

[11]B. Gellert and B. Kronast, Appl. Phys. B **32**, 175 (1983).

[12]J. E. Bernard, H. A. Baldis, D. M. Villeneuve, and K. Estabrook, Phys. Fluids **30**, 3616 (1987).

[13]J. E. Bernard, H. A. Baldis, D. M. Villeneuve, and A. B. Langdon, Phys. Rev. Lett. **58**, 1644 (1987).

[14]W. Rozmus, Y. Al-Shiraida, and A. A. Offenberger, Phys. Fluids **27**, 589 (1984).

[15]W. Rozmus, W. Tighe, A. A. Offenberger, and K. Estabrook, Phys. Fluids **28**, 920 (1985).

[16]K. Nishikawa, J. Phys. Soc. Jpn. **24**, 1152 (1968).

[17]W. L. Kruer, P. K. Kaw, J. M. Dawson, and C. Oberman, Phys. Rev. Lett. **24**, 987 (1970).

[18]K. Estabrook and W. L. Kruer, Phys. Fluids **26**, 1888 (1983).

[19]P. K. Kaw and J. M. Dawson, Phys. Fluids **12**, 2586 (1969).

[20]D. F. Dubois and M. V. Goldman, Phys. Rev. **164**, 207 (1967).

[21]J.-N. Leboeuf and T. W. Johnston, Can. J. Phys. **53**, 2387 (1975).

[22]C. Oberman and G. Auer, Phys. Fluids **17**, 1980 (1974).

[23]L. Spitzer, Jr., *Physics of Fully Ionized Gases* (Interscience, New York, 1962).

[24]Y. S. Al-Shiraida and A. A. Offenberger, Phys. Fluids **30**, 593 (1987).

[25]W. M. Manheimer and D. G. Colombant, Phys. Fluids **21**, 1818 (1978).

[26]L. M. Gorbunov, Zh. Eksp. Teor. Fiz. **55**, 2298 (1968) [Sov. Phys.–JETP **28**, 1220 (1969)]; J. Drake, P. K. Kaw, Y. C. Lee, G. Schmidt, C. S. Liu, and M. N. Rosenbluth, Phys. Fluids **17**, 778 (1974); W. Manheimer and E. Ott, *ibid.* **17**, 1413 (1974).

[27]P. K. Kaw and J. M. Dawson, Phys. Fluids **14**, 792 (1971).

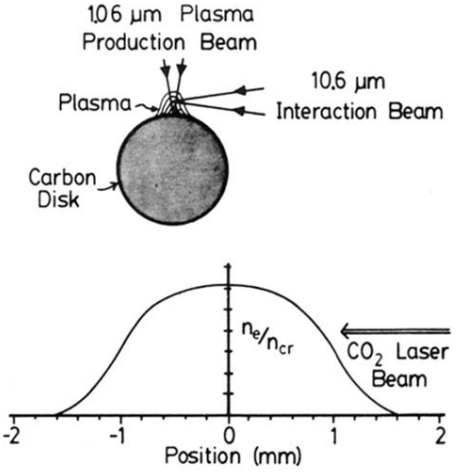

FIG. 4. Experimental arrangement showing the disk target and the plasma production and interaction laser beams. The graph shows a typical plasma density profile along the axis of the CO_2 laser beam.

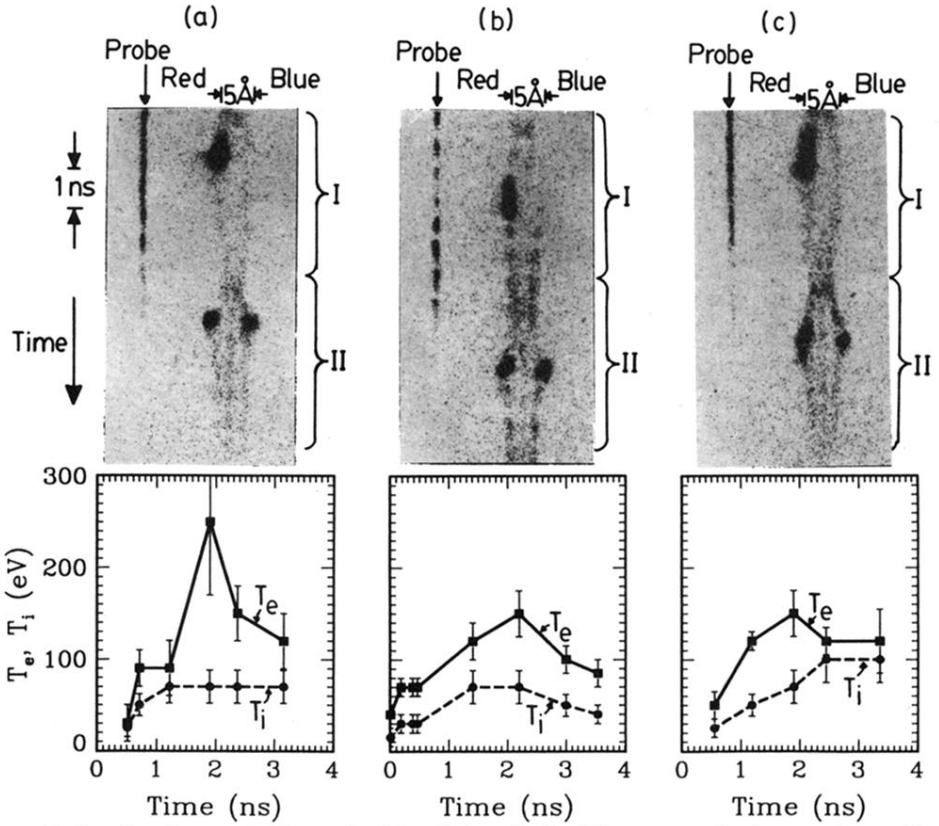

FIG. 7. Streak records showing the spectrally resolved ion feature in the Thomson scattering spectrum. I is the spectrum from fluctuations which propagated perpendicular to $\mathbf{v}_{osc}$ (parallel to $\mathbf{k}_0$). II is the spectrum from fluctuations which propagated parallel to $\mathbf{v}_{osc}$. The graphs show the electron and ion temperature time histories determined from best fits of the upper spectrum (I) by theoretical scattering spectra. (a) $0.6n_{cr}$, 25 J; (b) $0.6n_{cr}$, 23 J; (c) $0.7n_{cr}$, 22 J.